




Effect of Air Atmosphere Sensitization on Formation of PbSe p - n Junctions for High-Performance Photodetectors

SHUNYA YAN,^{1,2} QI YANG,¹ SHUANGLONG FENG,¹ JUN SHEN,¹
JUN YANG,¹ LINLONG TANG,¹ CHONGQIAN LENG,¹
and DAHUA ZHOU ^{1,3}

1.—Chongqing Key Laboratory of Multi-Scale Manufacturing Technology, Chongqing Institute of Green and Intelligent Technology, Chinese Academy of Sciences, Chongqing 400714, China. 2.—School of Physical Science and Technology, MOE Key Laboratory on Luminescence and Real Time Analysis, Southwest University, Chongqing 400715, China. 3.—e-mail: zhoudahua@cigit.ac.cn

Photodetectors based on polycrystalline lead salts are widely used to detect light in the mid-infrared range because they can be used at room temperature. In their fabrication, the sensitization process is considered to be the most critical factor. In this work, the crystalline structure of PbSe films deposited by electron-beam evaporation was analyzed by scanning electron microscopy, x-ray diffraction, and x-ray photoemission spectroscopy. The results showed that lead oxides were formed during the annealing process. We also investigated the electrical properties of the samples by Hall-effect measurements. In photodetection experiments at room temperature, the PbSe-based photodetectors showed responsivity and detectivity of 0.16 A/W and 6.66×10^8 cm Hz^{1/2}/W, respectively. Remarkably, we measured a photocurrent even without applying a bias voltage, which implies that the p - n junctions separate the carriers in these films, thus also proving the existence of micro p - n junctions in the film. A carrier separation model is proposed to describe the conduction process.

Key words: PbSe, infrared detector, sensitized mechanism, p - n junction

INTRODUCTION

Due to its absorption band in the range from 3×10^{-6} m to 5×10^{-6} m, lead selenide (PbSe) is a typical group IV–VI semiconductor used in infrared detectors.^{1–3} In particular, its low cost, room-temperature operation, and high detectivity make it a very interesting and widely investigated compound for the realization of photosensitive layers.

PbSe films can be prepared by various methods, such as chemical bath deposition (CBD), physical vapor deposition, molecular beam epitaxy, and pulsed laser deposition; For example, PbSe films have been obtained by electrochemical deposition⁴

and by the CBD technique.⁵ However, notwithstanding the deposition method applied, PbSe films must be subject to further thermal treatment in a specific atmosphere, a process usually referred to as sensitization. Sensitization usually plays a crucial role in determining the properties of PbSe-based photodetectors, and much effort has been devoted to investigation and optimization of the corresponding experimental procedures and theoretical analysis.

An explanation widely used for the enhanced sensitivity of Pb–Se film is based on the assumption that O²⁻ in the PbSe cell plays the role of minority-carrier traps, thus forbidding recombination of e - h pairs and increasing the lifetime of majority carriers.⁶ Other models assume that potential barriers are formed between n - and p -type regions during the sensitization process, since electrons and holes are trapped in their corresponding areas, such that

(Received November 18, 2019; accepted May 11, 2020;
published online May 27, 2020)

the mobility is highly increased under infrared irradiation.⁷ Zhao et al. have also introduced a charge separation model to explain the mechanism of enhanced photoconductivity of polycrystalline lead salt photoconductors.⁸ However, the sensitization effect and photoconductive mechanism are rather involved, especially when iodine is employed in the sensitization process,⁹ and several open questions remain regarding the true nature of the photoconductivity observed in lead chalcogenide thin films.

We report herein a study on PbSe films prepared by electron beam evaporation (EBE) on Si/SiO₂ substrate, then annealed in air atmosphere. Successful sensitization was confirmed by x-ray photoemission spectroscopy (XPS) and x-ray diffraction (XRD) measurements. The electrical parameters of the film, including the carrier concentration, mobility, and resistance, were recorded by Hall-effect measurements. Finally, we carried out a series of photodetection experiments and found that operation at higher temperature enhanced the photoresponsivity. In particular, we found that, under infrared irradiation, a photocurrent may be observed also without a bias voltage. Based on these results, a model of micro *p-n* junctions is proposed to describe the sensitization and carrier separation processes. To the best of the authors' knowledge, this is the first time that photoconductivity in PbSe film has been observed at zero bias voltage, a result that also suggests the presence of *p-n* junctions within the film.

EXPERIMENTAL PROCEDURES

In the first stage, we realized electrodes by depositing Cr/Au (3×10^{-9} m/ 50×10^{-9} m) on the substrate. Then, using the EBE technique, a PbSe film ($\sim 1 \times 10^{-6}$ m thickness) was deposited on the substrate. The substrate was heated to 100 °C during the deposition process, and the film deposition rate was 2 Å/s to 3 Å/s at pressure of $\sim 5.0 \times 10^{-4}$ Pa. The strips and electrodes were all formed using a lift-off process. Finally, the sensitization process was carried out in air by leaving the sample for 1 h at a temperature in the range from 200 °C to 600 °C. The crystal structure of the PbSe films was studied by XRD analysis using Cu K_α radiation (X'Pert3 Powder, Analytical B.V, $\lambda = 1.5418$ Å) in the 2θ scan range from 10° to 70°. Meanwhile, scanning electron microscopy (SEM, JSM-7800F; JEOL) was used to investigate the surface morphology, and x-ray photoelectron spectroscopy (XPS, ESCALAB250Xi; Thermo Fisher Scientific) to identify the film's components (Pb, Se, and O). Hall measurements were carried out to determine various electrical parameters, such as the Hall coefficient, carrier mobility, and concentration. A Keithley 4200 semiconductor characterization system was used to evaluate the photoresponse at room temperature, and the

response time was recorded by means of a Keithley 7510 system.

RESULTS AND DISCUSSION

SEM images of the samples annealed at different temperatures are shown in Fig. 1. Figure 1a shows a surface image of the as-grown sample, which consists of compact, small worm-like structures and a smooth cubic-shaped crystalline structure. The morphology of the films annealed at temperatures from 200 °C to 600 °C for 1 h is shown in Fig. 1b–f. These results reveal that the crystallite size increased with temperature while the film surface became more compact, forming a dense microstructure after annealing at higher temperatures.

XRD patterns (Fig. 2) were then used to analyze the crystalline structure of each sensitized film. The most intense diffraction peak for the as-deposited film was observed at 29.1°, indicating a predominant growth direction of the crystallites of (200). This is likely due to the fact that the (200) direction has lower interface energy (compared with other directions), consisting of the rod-like grains shown in Fig. 1a.⁹ The peaks located at 41.6°, 49.2°, and 60.3° are due to PbSe (220), (311), and (400), indicating that the as-grown film was PbSe according to Joint Committee on Powder Diffraction Standards (JCPDS) card no. 78-1903. After thermal treatment of the samples, several peaks due to oxides (such as PbO, PbSeO₃) appeared, and their intensity increased with temperature. When the samples were treated at 200 °C to 400 °C, rock-salt PbSe phase was still dominant, even though the related oxide peaks became more relevant with increasing temperature, indicating that the PbSe cell was covered by a layer of oxides. When the temperature was increased to 500 °C and 600 °C, the PbSe (200) peaks were replaced by PbSeO₃ (002) and (400) peaks. Meanwhile, other peaks due to PbSeO₄, PbO, and SeO₂ also started to appear, indicating that, at higher temperatures, the original PbSe film was oxidized.

XPS measurements were carried out to characterize the chemical states of the constituent elements in both the as-grown and annealed PbSe films. The Pb 4*f* spectra of the as-grown film is shown in Fig. 3a, revealing two clear transitions at binding energy of about 137 eV and 142 eV, which correspond to the Pb 4*f*^{7/2} and Pb 4*f*^{5/2} diffraction peaks. The transitions at 138.3 eV (Pb 4*f*^{7/2}) and 143.3 eV (Pb 4*f*^{5/2}) can be assigned to Pb²⁺ in PbO, whereas the Pb 4*f*^{7/2} and Pb 4*f*^{5/2} transitions at 137.1 eV and 142.0 eV correspond to Pb²⁺ in PbSe. However, for the film annealed at 400 °C for 1 h, only the Pb 4*f*^{7/2} and Pb 4*f*^{5/2} transitions at 138.3 eV and 143.3 eV were observed, corresponding to Pb²⁺ in PbO.¹⁰ The Se 3*d* XPS spectrum of the as-grown film is shown in Fig. 3b. One can observe the transitions at 53.0 eV and 53.9 eV corresponding to Se²⁻ in PbSe alloy, the transitions at 54.5 eV and

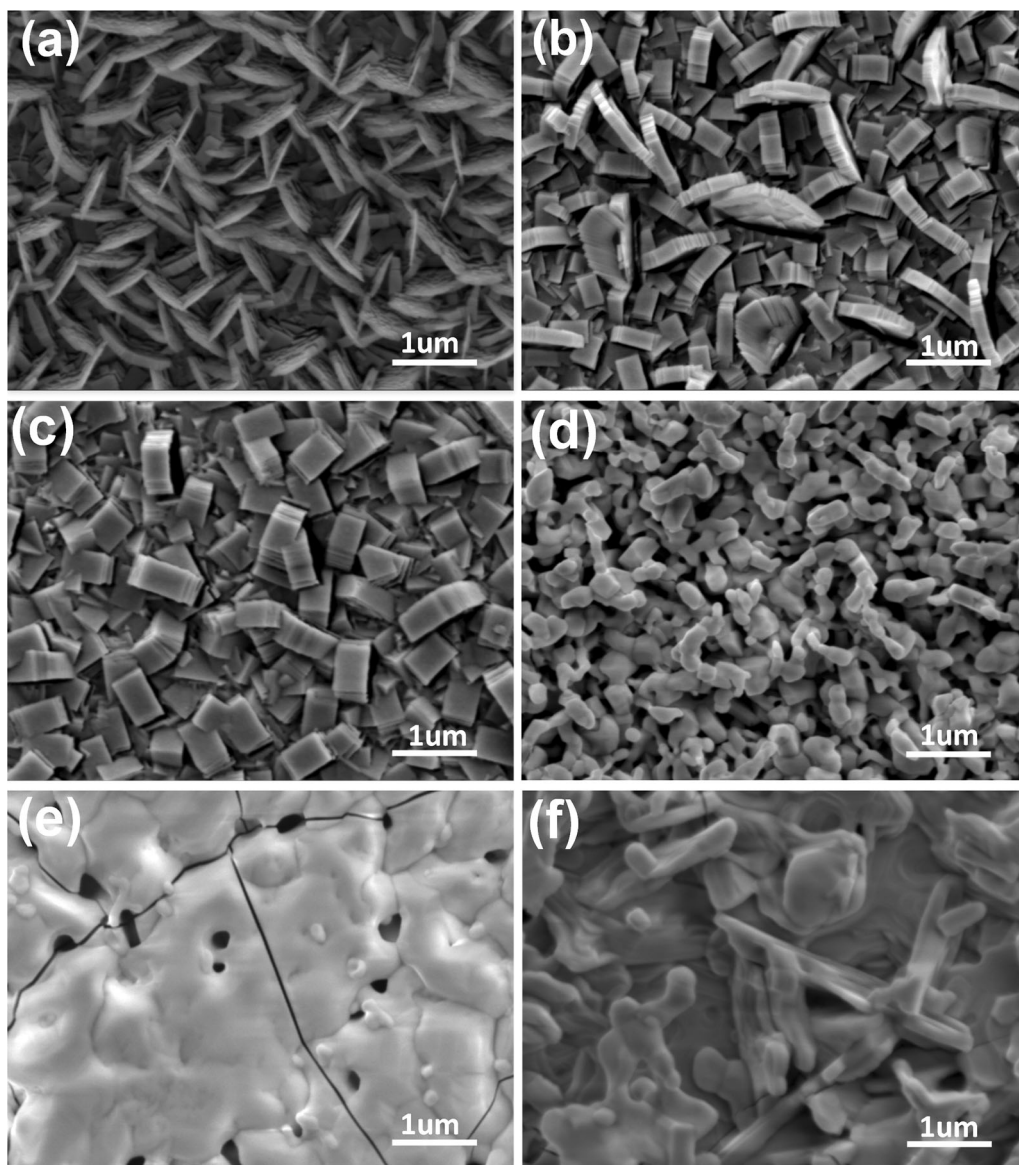


Fig. 1. SEM images of as-grown and annealed PbSe films: (a) as-grown film, and annealed at (b) 200 °C, (c) 300 °C, (d) 400 °C, (e) 500 °C, and (f) 600 °C.

55.4 eV due to pure Se, and the transitions at 58.3 eV and 59.2 eV due to Se^{4+} in SeO_2 . However, the transitions due to Se^{2-} in PbSe and Se element cannot be observed for the sample treated at 400 °C. These XPS results illustrate that the treated films were covered by PbSeO_3 resulting from the reaction of PbO and SeO_2 during the surface passivation process.^{8,11–14} As suggested in Ref. 15, the formation of oxide compounds means that Pb–Se bonds are broken while Pb–O and Se–O bonds are formed instead. Such reactions are thermodynamically favored because the dissociation energy of Pb–Se (302 kJ/mol) is lower than that of Pb–O (382 kJ/mol) or Se–O (464 kJ/mol). Therefore, as the annealing temperature is increased, the film surface is gradually oxidized, until reaching total oxidization at 500 °C.

To understand the variation of the electrical properties as a function of annealing temperature, Hall measurements were carried out to evaluate the carrier concentration, mobility, and resistance of the films; the results are shown in Fig. 4. Figure 4a reveals that the carrier concentration in the film decreased from $3.6 \times 10^{19} \text{ cm}^{-3}$ to $1.7 \times 10^{18} \text{ cm}^{-3}$ when the annealing temperature was increased to 250 °C. The carrier concentration further decreased to $9.0 \times 10^{17} \text{ cm}^{-3}$ at 300 °C, and eventually dropped to $7.0 \times 10^{16} \text{ cm}^{-3}$ at 400 °C, being about 1/500th of the value for the as-grown film. This dramatic decrease of the carrier concentration below 250 °C is due to evaporation of Se from the PbSe surface, which is not quantitatively compensated by the oxygen diffusing into the film. Furthermore, the acceptor defects are reduced during

the sensitized process as the defects in the film are passivated.¹⁶

The carrier mobility in the PbSe films is shown in Fig. 4b, where one can see a significant increase

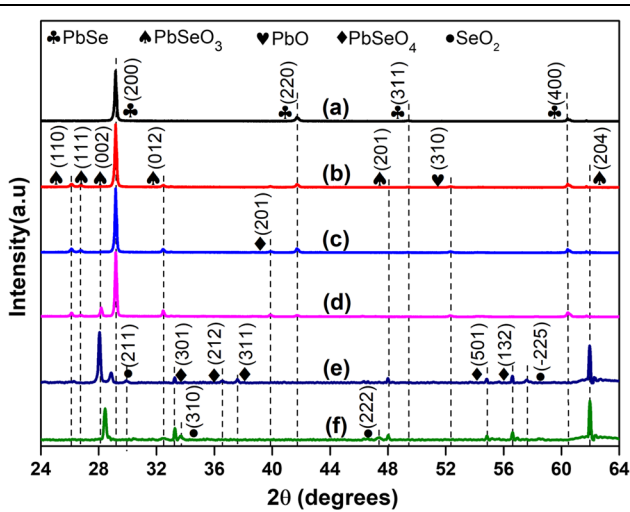


Fig. 2. XRD patterns of PbSe films (a) as-grown, and annealed at (b) 200 °C, (c) 300 °C, (d) 400 °C, (e) 500 °C, and (f) 600 °C.

from 5.9 cm²/V-s (as grown at room temperature) to 16 cm²/V-s (after annealing at 300 °C) to a maximum value of 29.6 cm²/V-s (after annealing at 400 °C), which is five times higher than the value for the as-grown film. This phenomenon can be attributed to the oxygen atoms diffusing into the PbSe film and occupying some Se vacancies, thus passivating dislocations and reducing the carrier trapping. At the same time, the increase of the grain size with temperature, as well as the reduction of the grain boundaries, also contribute to the increase in the mobility.

As shown in Fig. 4c, the resistance also changed as a function of annealing temperature, increasing slowly from 0.029 Ω cm in the as-grown film at room temperature to 0.415 Ω cm after annealing at 300 °C. After annealing at temperatures above 350 °C, the curve became steeper and the value after annealing at 400 °C was about 2.5 times higher than that after annealing at 350 °C. We conclude that, at 400 °C, the oxide layer of the film became thicker and the resistance of grain boundaries increased greatly, so the resistance increased as well, despite the carrier mobility achieving its maximum value and the carrier concentration its minimum.¹⁶

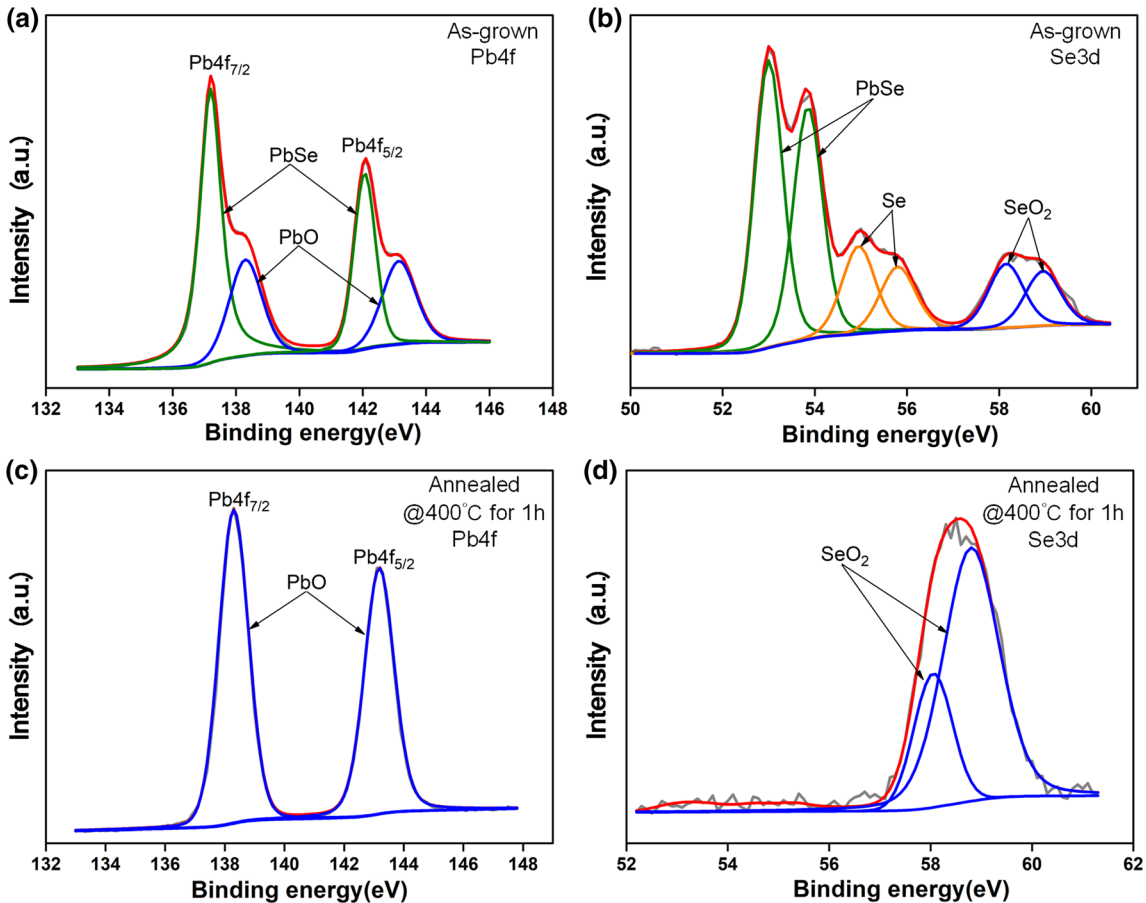


Fig. 3. (a, c) Pb 4f and (b, d) Se 3d XPS spectra of PbSe films (a, b) as-grown and (c, d) annealed at 400 °C for 1 h.

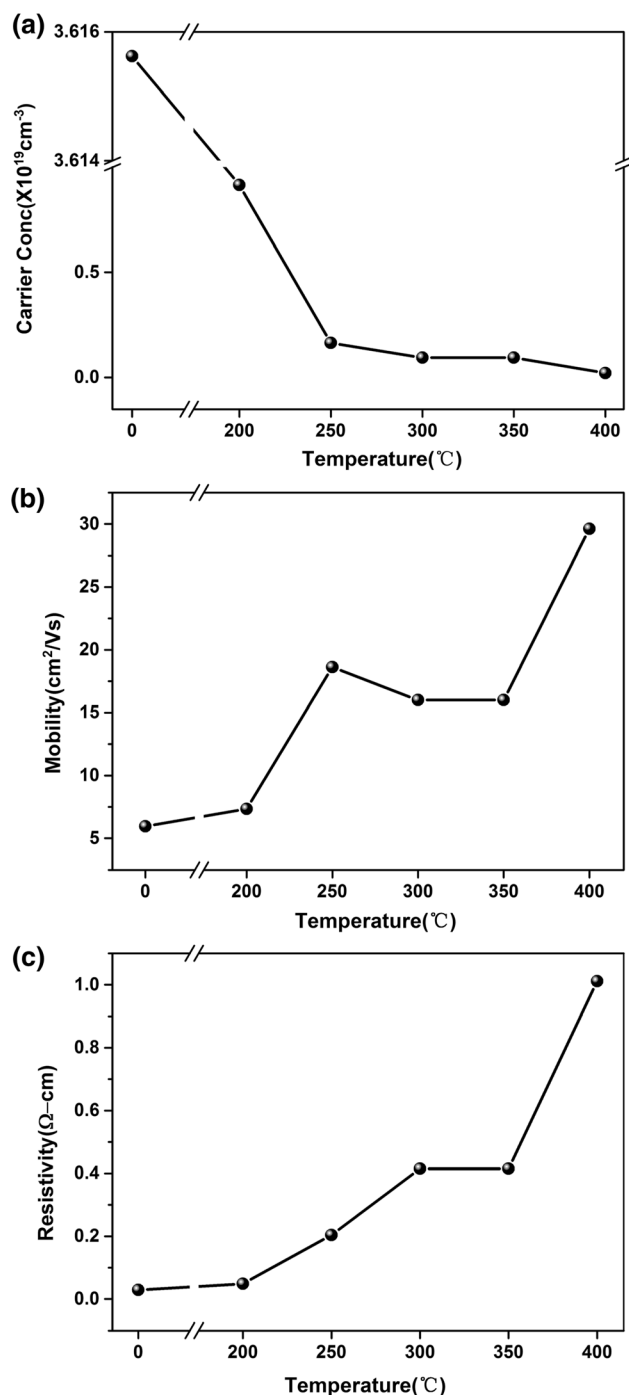


Fig. 4. (a) Carrier concentration, (b) mobility, and (c) resistivity versus annealing temperature.

The photosensitivity performance was determined by measuring the photocurrent of the devices; the results are shown in Fig. 5. The photoconductivity of these samples was investigated using a focused 2.7- μm laser beam with spot area of about 1 mm². In particular, we measured the photocurrent with a bias voltage of 30 V, laser power of 5×10^{-4} W, and on/off cycles of the chopped infrared illumination of 10 s. To assess the performance of the devices, we employed the

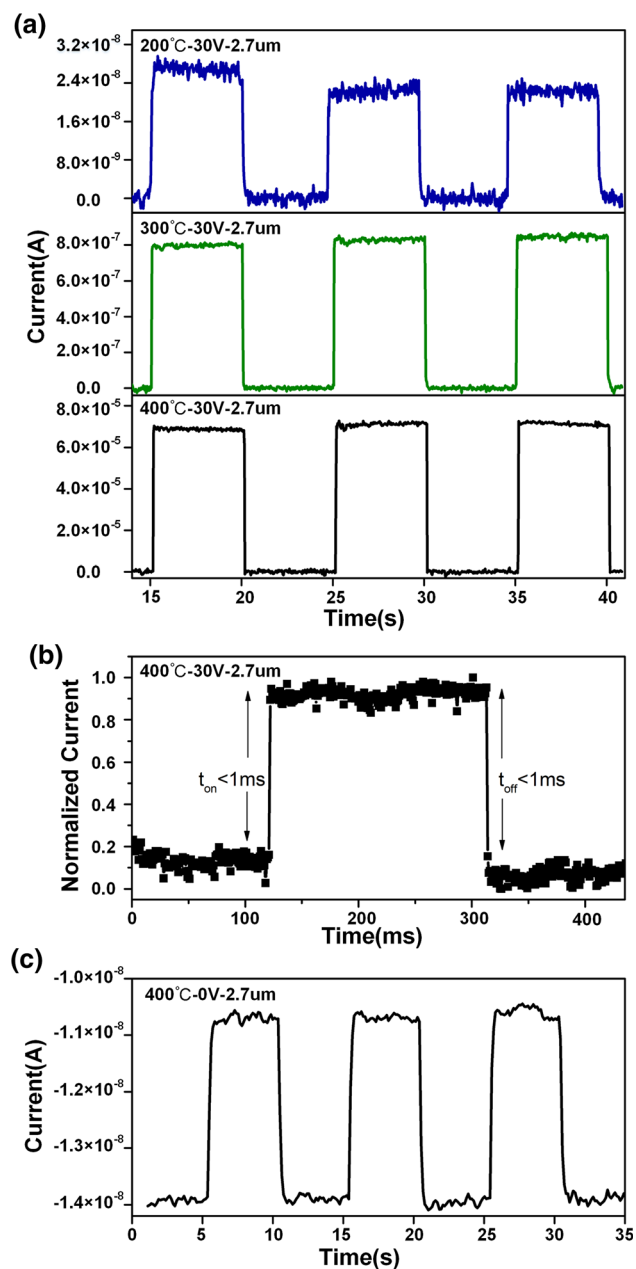


Fig. 5. (a) Photocurrent response curves to 2.7- μm light with bias voltage of 30 V; (b) Transient response of PbSe film annealed at 400 °C; (c) Photocurrent response at zero bias voltage of film annealed at 400 °C.

responsivity and detectivity at fixed incident optical power and bias voltage. The definition of the photoresponsivity (R) is $R = I_{\text{ph}}/P$, where I_{ph} is the photocurrent and P is the optical power of the incident infrared radiation.¹⁷ The results indicated that the device annealed at 400 °C showed the highest responsivity and detectivity, with values of 0.16 A/W and $6.7 \times 10^8 \text{ cm Hz}^{1/2}/\text{W}$, respectively. The full set of results are presented in Table I. The detectivity (D^*) is defined as $D^* = R \times (A/2qI_{\text{dark}})^{1/2}$, where A is the sensitive area of the photodiode, q is the absolute value of the electron charge

Table I. Photoresponsivity R (mA/W) and detectivity D^* (cm Hz^{1/2}/W) of PbSe film at different bias voltages for 2.7- μ m laser radiation

	Temperature/bias voltage			
	200 °C/30 V	300 °C/30 V	400 °C/30 V	400 °C/0 V
R	0.1	1.7	160	6.6×10^{-3}
D^*	1.94×10^7	2.93×10^7	6.66×10^8	1.13×10^7

(1.6×10^{-19} C), I_{dark} is the dark current, and R is the responsivity.^{17,18} For the different devices, we measured detectivity at 2.7 μ m are 1.94×10^7 cm Hz^{1/2}/W (after annealing at 200 °C), 2.93×10^7 cm Hz^{1/2}/W (after annealing at 300 °C), and 6.66×10^8 cm Hz^{1/2}/W (after annealing at 400 °C), as shown in Table I. The D^* and R values increased with annealing temperature because of the greater chance of oxidizing the PbSe particles at higher temperature, forming p - n junctions consisting of a core-shell structure of the oxide layer and PbSe. As also shown by the time-resolved photoreponse in Fig. 5a, the film device annealed at 400 °C exhibited high reproducibility and low dark current with the light on and off. In Fig. 5b, a response on the order of milliseconds can be observed. It is worth noting that the photodetector produced a photocurrent response to infrared radiation even without a bias voltage. This is shown in Fig. 5c, which reveals a photoresponsivity and detectivity of 6.6×10^{-6} A/W and 1.13×10^7 cm Hz^{1/2}/W, respectively.

As mentioned in the “Introduction,” the photoconductive mechanism of lead salt films is not yet fully understood.^{19–21} Previous models of the sensitization mechanism were based on specific results, whereas direct evidence is not available. In this work, we observed that the surface of p -type polycrystalline PbSe can be quickly converted to n -type during the applied process, even without extra oxygen.²² This produces p - n junctions in the film, leading to the detection of a photoreponse even at zero bias voltage. Additionally, the conversion of the PbSe surface to PbO and PbSeO₃ was confirmed by XRD analysis and XPS, which were in full agreement with previous results regarding the formation of an n -type outer shell.²³ Under infrared illumination, photoinduced e - h pairs are spatially separated by the built-in potential, and this spatial separation may enhance the carrier lifetime and effectively inhibit their recombination, such that the photoconduction of polycrystalline PbSe is improved after sensitization.

Based on such a carrier separation model, the results of our experiments can be explained coherently as follows: At first, the film starts to oxidize after being treated at 200 °C (Fig. 6b), and the n -type oxide layer wraps a small part of the p -type PbSe particles. When the temperature is increased to 400 °C, the oxidation level increases as well, and the n -type layer becomes

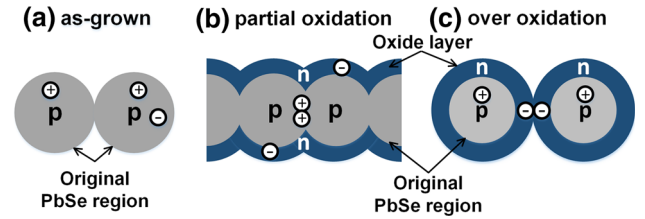


Fig. 6. Schematic of PbSe grain oxidation process during treatment: (a) the as-grown film is p -type, and e - h pairs are not separated effectively. (b) The PbSe core is covered by an oxide layer (n -type), then the e - h pairs are separated by the built-in electric field and the transport in n and p channels. (c) The holes cannot pass through, due to the thick oxide layer.

thicker, since more PbSe particles are wrapped by the oxide layer. The photogenerated carriers are thus effectively separated and an enhanced conductivity is achieved. If the temperature is increased above 500 °C, the resistance becomes too high, and the film becomes nonconductive since the conducting channels are closed by oxides (Fig. 6c). Indeed, Fig. 1e, f confirms that particles of the surface had melted, such that the photoconductive performance was dramatically deteriorated.

CONCLUSIONS

We fabricated PbSe films by electronic beam evaporation and annealed them in a closed environment without extra oxygen. With increasing annealing temperature, an increasing number of diffraction peaks due to oxides appeared in the XRD spectra, revealing an increase in the degree of oxidation. Compared with the as-grown film, the mobility and resistance of the annealed films increased, whereas the carrier concentration of the film annealed at 400 °C decreased. These results confirm that defect and dislocation passivation caused by oxygen reaction and diffusion may contribute to the improvement of the electrical properties of such films. Importantly, the photoreponse observed for the devices even at 0 V confirmed the formation of p - n junctions after sensitization, which improves the efficiency of carrier separation. These results and evidence may contribute to better understanding of the photoconductive mechanism of lead salt materials during and after sensitization.

ACKNOWLEDGMENTS

This work was supported by the National Nature Science Foundation of China (61704172) and the Venture & Innovation support Program for Chongqing Overseas Return (cx2018153).

REFERENCES

1. J.S.U.K. Mishra, *Semiconductor Device Physics and Design* (Berlin: Springer, 2008).
2. E.D. Palik, *Handbook of Optical Constants of Solids* (New York: Academic, 1998).
3. F.W. Wise, *Acc. Chem. Res.* 33, 773 (2000).
4. N. Mukherjee and A. Mondal, *J. Electron. Mater.* 39, 1177 (2010).
5. E. Barrios-Salgado, M.T.S. Nair, P.K. Nair, and R.A. Zingaro, *Thin Solid Films* 519, 7432 (2011).
6. J.N. Humphrey and R.L. Petritz, *Phys. Rev.* 105, 1736 (1957).
7. J.C. Slater, *Phys. Rev.* 103, 1631 (1956).
8. L. Zhao, J. Qiu, B. Weng, C. Chang, Z. Yuan, and Z. Shi, *J. Appl. Phys.* 115, 084502 (2014).
9. X. Sun, K. Gao, X. Pang, H. Yang, and A.A. Volinsky, *Thin Solid Films* 592, 59 (2015).
10. C. Gautier, M. Cambon-Muller, and M. Averous, *Appl. Surf. Sci.* 141, 157 (1999).
11. R.L. Petritz, *Phys. Rev.* 104, 1508 (1956).
12. S. Horn, D. Lohrmann, P. Norton, K. McCormack, and A. Hutchinson, *Infrared Technol. Appl.* XXXI, Pts 1 and 2 5783, 401 (2005).
13. H. Yang, L. Chen, X. Li, and J. Zheng, *Mater. Lett.* 169, 273 (2016).
14. F. Zhao, S. Mukherjee, J. Ma, D. Li, S.L. Elizondo, and Z. Shi, *Appl. Phys. Lett.* 92, 211110 (2008).
15. V.V. Tomaev, L.L. Makarov, P.A. Tikhonov, and A.A. Solomennikov, *Glass Phys. Chem.* 30, 349 (2004).
16. S. Zheng, J. Cheng, and J. Zheng, *Semicond. Optoelectron.* 37, 223 (2016).
17. S. Masala, V. Adinolfi, J.P. Sun, S. Del Gobbo, O. Voznyy, I.J. Kramer, I.G. Hill, and E.H. Sargent, *Adv. Mater.* 27, 7445 (2015).
18. X. Gong, M. Tong, Y. Xia, W. Cai, J.S. Moon, Y. Cao, G. Yu, C.L. Shieh, B. Nilsson, and A.J. Heeger, *Science* 325, 1665 (2009).
19. J. Chen, Y. Huang, N. Zhang, H. Zou, R. Liu, C. Tao, X. Fan, and Z.L. Wang, *Nat. Energy* 1, 16138 (2016).
20. N. Zhang, J. Chen, Y. Huang, W. Guo, J. Yang, J. Du, X. Fan, and C. Tao, *Adv. Mater.* 28, 263 (2016).
21. L. Zhang, G. Cheng, J. Chen, L. Lin, J. Wang, Y. Liu, H. Li, and Z.L. Wang, *Adv. Energy Mater.* 5, 1501152 (2015).
22. H. Yang, L. Chen, J. Zheng, K. Qiao, and X. Li, *Appl. Phys. A* 122, 710 (2016).
23. M.C. Torquemada, M.T. Rodrigo, G. Vergara, F.J. Sanchez, R. Almazan, M. Verdu, P. Rodriguez, V. Villamayor, L.J. Gomez, M.T. Montojo, and A. Munoz, *J. Appl. Phys.* 93, 1778 (2003).

Publisher's Note Springer Nature remains neutral with regard to jurisdictional claims in published maps and institutional affiliations.